RMetS
Royal Meteorological Society

Impact of climate change on urban heat island effect and extreme temperatures: a case-study

D. A. Sachindra,* A. W. M. Ng, S. Muthukumaran and B. J. C. Perera
Institute for Sustainability and Innovation, College of Engineering and Science of Victoria University, Melbourne, Australia

*Correspondence to: D. A. Sachindra, College of Engineering and Science, Victoria University, Footscray Park Campus, PO Box 14428, Melbourne, Victoria 8001, Australia. E-mail: sachindra.dhanapalaarachchige@vu.edu.au

This study investigated the impacts of climate change on the urban heat island (UHI) and the number of very hot (maximum temperature >35°C) and very cold days (minimum temperature <5°C) in the central business district (CBD) of Melbourne city in Australia. A station located in Laverton (less urbanised area), which is 17 km southwest of Melbourne CBD, was selected as the reference station for the computation of UHI intensity in Melbourne CBD. Using daily minimum/maximum temperatures at the two stations, nocturnal/diurnal UHI intensities in Melbourne CBD were computed for the period 1952–2010. It was found that in Melbourne CBD, nocturnal UHI intensities show a clear rising trend over the period 1952–2010 unlike the diurnal UHI intensities. For the analysis of nocturnal UHI intensities in Melbourne CBD, under changing climate, for each calendar month statistical models based on the gene expression programming (GEP) technique were developed for downscaling general-circulation model (GCM) outputs to monthly average minimum temperature at Melbourne CBD and Laverton. Using the outputs of HadCM3, GFDL2.0 and ECHAM5 pertaining to the A2 greenhouse gas emission scenario on the downscaling models, projections of monthly average minimum temperature were produced for the two stations over the period 2000–2099. In each season, at both stations, the ensemble average of monthly minimum temperature gradually increased over the period 2000–2099. The ensemble-average UHI intensity in Melbourne CBD projected into the future was higher for all seasons in comparison to that of period 1952–1971. Downscaling models based on the GEP technique were developed for each calendar month for projecting the number of very hot days in November–March and very cold days in May–September in Melbourne CBD. It was found that, in the future, summer weather will spread to early autumn, and winter weather will move to early spring, in Melbourne CBD.

Key Words: urban heat island; greenhouse gas; statistical downscaling

Received 15 July 2014; Revised 30 March 2015; Accepted 17 July 2015; Published online in Wiley Online Library 14 September 2015

1. Introduction

With rising greenhouse gas concentrations in the atmosphere, global climate has shown signs of change (McCarthy, 2009). Rise in surface air temperature, changes in spatio-temporal patterns of precipitation, increase in frequency of extreme events such as droughts and floods are some of the indications of changing climate. However, the elevation of surface air temperature is regarded as the most obvious change in the global climate (Jones *et al.*, 1986). According to the Intergovernmental Panel on Climate Change (IPCC), the rise in surface air temperature will tend to continue in the future with the greenhouse gas (GHG) emissions (IPCC, 2007). Elevated temperature causes an increase in the mortality rate in humans (Hajat *et al.*, 2010) as at high temperatures the central nervous thermoregulatory system of the human body fails to operate (Jay and Kenny, 2010).

In general, in urban environments, the temperature is observed to be higher in comparison to that at nearby rural areas. This phenomenon is called the urban heat island (UHI) effect (Oke, 1987; Arya, 2001). The space which surrounds the urban environment and shows higher temperatures in comparison to those in nearby rural areas is called the urban heat island. There are two main types of UHI effect: (i) atmospheric UHI effect and (ii) surface UHI effect (EPA, 2013). The elevated air temperature in urban areas in comparison to that of rural areas is called the atmospheric UHI effect. This phenomenon is more pronounced at night or pre-dawn in winter (EPA, 2013), and its intensity is measured using the air temperature readings at urban and rural observation stations. During sunny days urban surfaces absorb more solar energy and become warmer than the moist and often shaded rural surfaces; this phenomenon is called the surface UHI effect. The intensity of this kind of UHI is measured using the land

skin-temperature measurements obtained from remote-sensing techniques (e.g. Jin, 2012; Peng *et al.,* 2012).

The main causes of the UHI effect are the high heat capacity of urban surfaces, trapping of heat among urban structures/geometry (e.g. urban canyons), low wind speeds across the urban areas, and anthropogenic heat generation (Yow, 2007). The intensity of the UHI effect depends on many factors: the size of the city and its structure (Oke, 1973), the thermal properties of the building materials (Oke, 1988), the weather conditions (e.g. winds can reduce the intensity of the UHI: Morris and Simmonds, 2000), and the nature of the activities performed in the city (e.g. industrial cities have high UHI intensities). The intensity of a UHI also varies spatio-temporally (Jin, 2012).

Elevated temperatures caused by UHIs directly influence the health and comfort of the residents of cities. Also, the UHI effect increases the intensity and duration of heatwaves, and hence increases the heat stress related mortality rates (Tan *et al.,* 2010). The increase in the use of energy for cooling is regarded as another consequence of the UHI effect.

Howard (1833) is regarded as the first to provide valid evidence of the UHI phenomenon. Since then, in the literature, it has been documented that the air temperature in urban centres is relatively higher and has increased more rapidly over time compared to that in surrounding rural areas. In a study by Akbari *et al.* (2001), it was stated that the maximum daily temperature and minimum daily temperature in Los Angeles (USA) have risen by several degrees compared to in its surroundings over the last century. They concluded that mitigation of the UHI effect can be achieved effectively by replacing darker surfaces in urban environments with high-albedo surfaces, and this will reduce the energy cost and also improve the urban air quality. Livada *et al.* (2007) studied the variability of air temperature in summer in the city of Athens in Greece, and commented that the number of hours with air temperature above 30°C in Athens has increased in the recent past. Giannopoulou *et al.* (2011) investigated the UHI effect in Athens and stated that the densely constructed areas with little green infrastructure are warmer than the surrounding regions. They also found that the diurnal maximum temperature can be used to predict the nocturnal maximum temperature and the number of hours with temperatures exceeding 30°C, which can be used in determining the energy requirement for cooling buildings during the night. Schlunzen *et al.* (2010) found that, during summer, the monthly average difference between minimum temperatures in Hamburg (Germany) and its surrounding rural areas is in the range of 2.5–2.9°C. In that study it was commented that spatial variations of UHI intensity in the city depend on the degree of greening, presence of water bodies such as rivers, groundwater and also the building density. Wilby *et al.* (2003) investigated the intensity of London's UHI and concluded that the frequency of intense UHI events tends to increase under changing climate. De Souza *et al.* (2012) studied the characteristics of the UHI of the city of Manaus in Brazil, using the hourly observations of minimum temperature, maximum temperature and relative humidity. They found that the minimum temperature and maximum temperature in Manaus are higher than those in nearby forested area throughout the year. Furthermore, they stated that the UHI effect is more pronounced during night-time in Manaus. Morris and Simmonds (2000) studied the relationships between various synoptic conditions and the intensity of the UHI of Melbourne (Australia), using daily mean-sea-level pressure data and observed temperature. In that study they found that the intensity of Melbourne's UHI is higher when anticyclonic conditions develop over the southeast coast of Australia. Torok *et al.* (2001) studied the variations of intensities of UHIs with respect to the population in Melbourne and towns of Hamilton, Colac, Camperdown and Cobden in Australia. It was found that the intensities of UHIs in the above Australian cities/towns are less than those of North American and European cities/towns which have similar populations.

The study of the UHI effect under changing climate is an important task as it enables the future planning and construction of cities in such a way that the thermal discomfort caused by the UHI effect can be minimised. However, for the purpose of projection of the UHI effect into the future, temperatures in the cities and the rural areas should be projected into the future. For this purpose the climatic projections produced by general-circulation models (GCMs) are used. GCMs are regarded as the most reliable tools for simulation of global climate hundreds of years into the future, considering various plausible scenarios of concentrations of atmospheric GHGs (Anandhi *et al.,* 2009). They are only capable of producing simulation of global climate at a coarse spatial resolution in the order of a few hundred kilometres. In other words, GCMs are unable to resolve subgrid-scale features such as topography, clouds and land use which influence much of the variance of climate at the catchment scale (Tisseuil *et al.,* 2010). Therefore, the outputs of GCMs cannot be directly used in catchment-scale climate impact studies, which in general need hydroclimatic data at fine spatial resolutions (Willems and Vrac, 2011). As a solution to the mismatch between the coarse-scale climate presented in GCM outputs and the catchment-scale climate, downscaling techniques have been developed (Chen *et al.,* 2010). Downscaling techniques have been classified into two groups: (i) dynamic downscaling (uses physics-based relationships between GCM output and catchment-scale hydroclimatic variables) and (ii) statistical downscaling (uses statistical relationships between GCM outputs and catchment-scale hydroclimatic variables). More details about dynamic and statistical downscaling techniques can be found in Fowler *et al.* (2007). Owing to the low computational cost and simplicity, statistical downscaling techniques such as artificial neural networks (ANN), support vector machine (SVM), relevance vector machine (RVM), multi-linear regression (MLR), nonhomogeneous hidden Markov chains (NHHM), weather classification techniques and weather generators have been widely used for downscaling of GCM outputs to catchment-scale temperature and other hydroclimatic variables (e.g. Raje and Mujumdar, 2010; Haberlandt *et al.,* 2014; Hassan *et al.,* 2014; Mares *et al.,* 2014; Sachindra *et al.,* 2014a, 2014b, 2014c).

In the study of UHIs under changing climate, downscaling techniques can be used for the determination of temperature at urban and rural regions using the global climate simulations produced by GCMs. Then the temperature projections produced into the future using the downscaling approaches at the catchment scale can be used to study the UHI phenomena under changing climate. Some examples for using statistical downscaling for producing catchment-scale temperature projections to study the UHI effect under changing climate are found in Giannaros *et al.* (2014), Hoffmann *et al.* (2012) and Zakšek and Oštir (2012).

Climate change due to rising GHG concentrations influences the UHI effect and its consequences (Hoffmann *et al.,* 2012). Therefore the study of impacts of climate changes on the UHI effect and the changes in the temperature regime such as the variations in the number of extremely hot and cold days in cities are of high importance. This enables the implementation of the UHI-effect mitigation measures such as green infrastructure and better planning of cities by using high-albedo materials for roofing and use of ponds and fountains for cooling outdoor spaces. These mitigation measures will aid in reducing the heat stress and the mortalities caused by the UHI effect. In this study, the impact of climate change on the intensity of the UHI in the central business district (CBD) of Melbourne city in Australia and the number of very hot and cold days in the city were investigated. The findings of this study will provide the basis for the mitigation measures for the UHI effect in the CBD of Melbourne and maintaining an acceptable level of thermal comfort in outdoor settings in the city under changing climate in the future. This will allow the reduction of the number of mortalities and hospitalizations due to extreme temperatures and will reduce the burden on the health-care system. According to the past literature, no study has been conducted to investigate the impact of climate change on the intensity of the UHI of Melbourne.

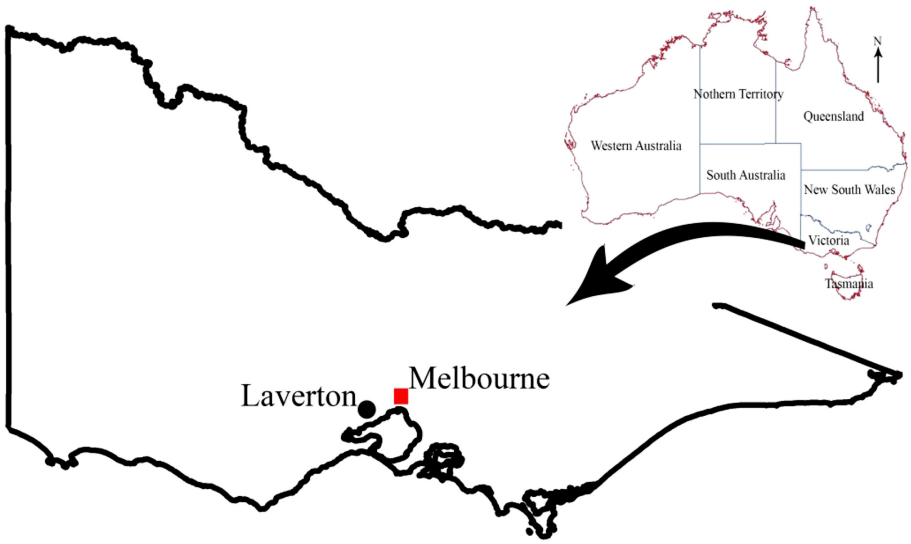

Figure 1. Location of Melbourne and Laverton in Victoria, Australia.

In this study, statistical models were developed at stations in the CBD of Melbourne and a nearby less urbanised area, for downscaling GCM outputs to air temperatures under changing climate, and hence the intensity of the UHI of Melbourne was projected into the future. Also, statistical models were used to project the number of very hot days in summer and number of very cold days in winter in the CBD of Melbourne into the future under changing climate.

2. Study area and data

The CBD of Melbourne in Victoria (Australia) is considered as the study area for this study. Melbourne, which is the commercial hub and the capital city of Victoria, is located in the southeastern region of the Australian mainland. The location of Melbourne is shown in Figure 1.

Many activities such as recreational, educational, administrative and commercial, attract large number of visitors into the city. The population of Melbourne in 2013 was about 4.25 million. The annual average precipitation in the CBD of Melbourne is about 650 mm. The average monthly minimum (maximum) temperature varies from 7.2 (14.1) °C in winter to 14.8 (25.1)°C in summer.

The weather observation station located in Melbourne city (station number 086071) at latitude 37.81°S (−37.81°) and longitude 144.97°E (at an altitude of 31 m from mean sea level) was selected as the representative station for the CBD of Melbourne. For the computation of UHI intensity in the CBD of Melbourne, as the reference gauge, the weather observation station located in Laverton (station number 087031) at latitude −37.86° and longitude 144.76° (at an altitude of 20 m from mean sea level) was selected. Laverton observation station is situated in a less urbanised area about 17 km southwest of Melbourne CBD. Morris and Simmonds (2000) used temperature data from the observation stations at Laverton, Melbourne airport, Moorabbin airport and Melbourne city for the computation of UHI intensity in the CBD of Melbourne. In that study, the average temperature from Laverton, Melbourne airport and Moorabbin airport were computed over the period 1973–1991 for representing temperature in rural settings.

In this study for the development of downscaling models for the projection of UHI intensity and number of very hot and very cold days, daily minimum and maximum temperature observations from the stations at Laverton and Melbourne were obtained from the Bureau of Meteorology, Australia, for the period 1952–2010. These daily data were used to derive the average monthly minimum (average computed from daily minimum temperatures) and maximum temperature (average computed from daily maximum temperatures) observations for each month for both stations. Throughout this article, the terms minimum temperature and maximum temperature refer to the average monthly minimum temperature and the average monthly maximum temperature respectively. Only the above two stations at Laverton and Melbourne were selected for this study due to the availability of a long record of observations with few missing data. The other two stations at Melbourne airport and Moorabbin airport considered in the study by Morris and Simmonds (2000) were not used in the present study, since the records of observations for the period 1952–1972 were not available at those stations.

For the calibration and validation of downscaling models for stations at Laverton and Melbourne, the National Centers for Environmental Prediction/National Center for Atmospheric Research (NCEP/NCAR) monthly reanalysis data for the period 1952–2010 were downloaded from http://www.esrl.noaa.gov/psd/. The twentieth-century climate experiment (20C3M) outputs of Hadley Centre Coupled Model - Version 3 (HadCM3), Geophysical Fluid Dynamics Laboratory Model - Version 2.0 (GFDL2.0) and European Centre Hamburg Model - Version 5 (ECHAM5) GCMs for the period 1952–1999 were downloaded from the Programme for Climate Model Diagnosis and Inter-comparison (PCMDI) (https://esgcet.llnl.gov:8443/index.jsp) for assessing the impact of GCM bias on the outputs of the downscaling models and its subsequent correction. According to Smith and Chandler (2009), HadCM3, GFDL2.0 and ECHAM5 are among the few GCMs capable of properly simulating the precipitation over Australia and El Niño/Southern Oscillation (ENSO). Also they argued that a GCM which can properly simulate the precipitation should be able to simulate other climatic variables with a good degree of accuracy. Therefore, HadCM3, GFDL2.0 and ECHAM5 were selected for the present study. The outputs of HadCM3, GFDL2.0 and ECHAM5 pertaining to the A2 greenhouse gas (GHG) emission scenario for the period 2000–2099 were downloaded from the same source for projecting the number of very hot and very cold days, temperature and hence UHI intensity in the CBD of Melbourne into the future. The A2 GHG emission scenario refers to high levels of GHG emissions due to the rapid economic growth of the world. The use of GCM outputs pertaining to the A2 GHG emission scenario enables the study of the UHI effect in Melbourne CBD under intense anthropogenic climate change.

3. Generic methodology

Statistical models were developed (calibrated and validated) for the urban station and the station located in a rural area

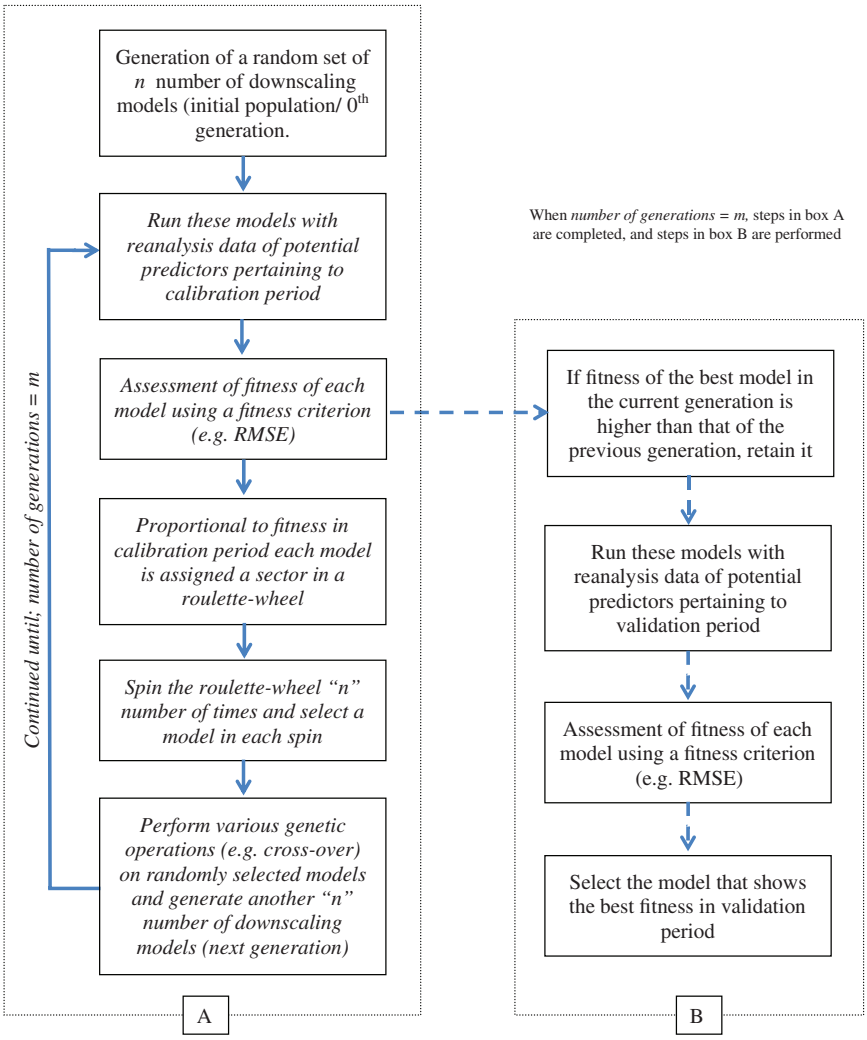

Figure 2. Main steps involved in the GEP-based downscaling model development.

for each calendar month for downscaling GCM outputs to average monthly minimum temperature. Another set of statistical models were developed for the urban station for each calendar month in summer and winter, for downscaling the GCM outputs to the number of very hot and cold days respectively. Development of separate downscaling models for each calendar month enables better capturing the seasonal variations of the predictor–predictand relationships. All downscaling models were developed using the gene expression programming (GEP) technique. The GEP technique was selected for developing the downscaling models in this study as it is capable of capturing the complex nonlinear relationships between the predictors and the predictand of interest (e.g. Hashmi *et al.*, 2011). Particularly the relationships between the predictors and the number of very hot and very cold days were assumed to be highly complex and nonlinear. Therefore a nonlinear regression technique such as GEP was considered to be suitable for this study.

3.1. Gene expression programming (GEP) based downscaling models

GEP is an evolutionary algorithm which mimics Darwin's theory of evolution. In GEP, initially a set of mathematical models (e.g. downscaling models) for relating the predictors with the predictand of interest are randomly generated and then they are evolved until their fitness/performance reaches a maximum or a predefined threshold or up to a predefined number of generations. The main steps involved in the GEP algorithm implemented in this study are shown in Figure 2. A more elaborated explanation of the GEP algorithm is found in Ferreira (2006).

Initially, a set of n number of downscaling models (e.g. 30 models) called the initial population (or the zeroth generation) is randomly generated. In this process, mathematical functions (e.g. $+$, $-$, $\times$, $/$) and constants are used to build relationships between the predictors and the predictand of interest. Then using the reanalysis data pertaining to the potential predictors as inputs to these n downscaling models, the values of the predictand over the calibration period are reproduced. Thereafter, the fitness (which can be measured using e.g. root-mean-square error) of each of the n downscaling models in the calibration period is measured. Then using the roulette-wheel selection as described below, n number of downscaling models are selected for genetic operations.

In roulette-wheel selection, a sector of the wheel is assigned to each individual downscaling model proportional to its fitness in calibration (i.e. models with higher fitness have a larger sector of the wheel). Fitness $F(I,j)$ of the ith downscaling model in the jth generation is computed using Eq. (1), where RMSE refers to the root-mean-square error of the ith downscaling model in the calibration period.

$$F(i,j) = \left|1 - \frac{1}{RMSE(i,j)}\right|. \quad (1)$$

Then the concept of spinning of the roulette wheel is used for the selection of the individual downscaling model. This process is repeated n number of times enabling the selection of n number of downscaling models (the same model can get selected several times). The roulette-wheel selection allows the models with higher fitness to have greater probability of selection. The selection probability $P(i,j)$ of the ith downscaling model in the jth

generation for the genetic operations in each spin of the roulette wheel is given by Eq. (2):

$$P(i,j) = \frac{F(i,j)}{\sum_{i=1}^{n} F(i,j)}. \quad (2)$$

Thereafter, genetic operations such as replication, mutation, transposition and recombination (cross-over) are performed on the above-selected downscaling models to produce a new set of n number of downscaling models called the first generation. For each of these genetic operations, downscaling models are randomly selected at predefined probabilities. Replication refers to the operation that involves copying a randomly chosen downscaling model in the current generation to the next generation. Mutation refers to the genetic operation that involves replacing a section of a randomly chosen downscaling model with another totally new section to generate a model for the next generation. Therefore, mutations introduce new genetic information to the next generation of downscaling models. In transposition, a part of a randomly chosen downscaling model is relocated to a different position in the model structure, yielding another downscaling model for the next generation. In recombination, two models in a certain generation are randomly chosen and some parts of these models are exchanged between them, creating two new daughter models for the next generation.

After application of genetic operations, using reanalysis data pertaining to the potential predictors as inputs to the n downscaling models (in the first generation), the values of the predictand corresponding to the calibration period are reproduced and the fitness of each downscaling model is quantified. The above procedure (see italicised text in Figure 2) is repeated m number of times (e.g. $m = 10\,000$) producing m number of model generations. The steps involved in the above procedure are shown in dotted box A in Figure 2.

With the production of each generation of models, the downscaling model that shows better fitness than the best downscaling model in the previous generation is retained (follow the dotted arrows in Figure 2). In other words, downscaling models that show increase in fitness in calibration are retained. Then, these downscaling models (retained in the previous step) are run with the reanalysis data pertaining to the potential predictors and the values of the predictand corresponding to the validation period are reproduced. The downscaling model that shows the best fitness in the validation period is selected as the best downscaling model (refer to steps in dotted box B in Figure 2), and the potential predictors used in that model are identified as the best potential predictors. The above procedure is repeated for each calendar month separately. This process yields the best downscaling model with the best set of potential predictors for each calendar month.

3.2. Calculation of urban heat island intensity

Nocturnal (during night-time) and diurnal (during daytime) atmospheric UHI intensities for each day for the urban city centre were calculated using Eq. (3) with the daily observations of minimum temperature and maximum temperature, respectively, at the urban and rural stations. The computation of nocturnal and diurnal UHI intensities enabled the identification of which of the two intensities is consistently high in the CBD of the city of interest. This identification enables the development of downscaling models (as described later) for the projection of either minimum temperature or maximum temperature for the consistently higher UHI intensity (e.g. if nocturnal UHI intensity is consistently higher then downscaling models are to be developed only for minimum temperature). In Eq. (3), $T_{(\text{urban})}$ and $T_{(\text{rural})}$ refer to the minimum temperature (or maximum temperature) at urban and rural station, respectively, in calculation of the nocturnal (or diurnal) UHI intensity at the urban city centre.

$$UHI_{\text{Intensity}} = T_{(\text{urban})} - T_{(\text{rural})}. \quad (3)$$

3.3. Atmospheric domain and predictor selection

For the extraction of large-scale atmospheric variables to develop downscaling models, an adequately large atmospheric domain was defined over the study area. An adequately large atmospheric domain allows the consideration of atmospheric processes influential on the climate at the points of interest. An overly large atmospheric domain increases the computation burden and also introduces noise to the downscaling models. The use of a very small atmospheric domain can cause the omission of some atmospheric circulations influential on the predictand of interest (Sachindra *et al.*, 2014a).

After the definition of the atmospheric domain, probable predictors were selected for minimum (or maximum) temperature for both stations based on past literature. The probable predictors are the variables most likely to influence the predictand of interest. Then for each calendar month, potential predictors were extracted from the pool of probable predictors. The potential predictors are subsets of probable predictors which vary from season to season as well as from one station to another, and they are the most influential variables on the predictand of interest. Potential predictors for each calendar month were selected separately, as the atmospheric circulations and hence the predictor–predictand relationships vary from season to season (Karl *et al.*, 1990). The selection of predictors for each calendar month enables building more robust downscaling models. For selection of potential predictors from the pool of probable predictors, the Pearson correlation coefficient was computed between the reanalysis data for probable predictors and the observations of minimum or maximum temperature at the urban and the rural stations for each calendar month. Then the probable predictors which showed statistically significant correlations (at 95% confidence level, $p = 0.05$) with observed minimum or maximum temperature for the past climate were selected as the potential predictors for each calendar month for each observation station.

3.4. Downscaling models for minimum or maximum temperature

In a study by Sachindra *et al.* (2014a), for different calendar months, 3–12 potential variables were used as inputs to a model developed for downscaling reanalysis outputs to monthly precipitation at a station in northwestern Victoria, Australia. In the current study, for the development of downscaling models at the urban and the rural stations the ten best potential predictors which showed statistically significant correlations (at 95% confidence level, $p = 0.05$) with observations of minimum (or maximum) temperature were selected for each calendar month. The selection of too few variables can cause the failure of the model to adequately explain the predictor–predictand relationships. On the other hand, the selection of too many variables can introduce redundant information to the model and can lead to over-fitting in model calibration and under-fitting in model validation.

In this study, reanalysis data for the ten best potential predictors and observations of minimum (or maximum) temperature for each calendar month at each station were split into two categories in chronological order. The first two-thirds of the data were allocated for the calibration of the downscaling models and the rest of the data were used for the validation of these models. The reanalysis data of potential predictors for both calibration and validation were standardised with their means and standard deviations pertaining to the calibration period. This was done by subtracting the mean from the data of each potential predictor, and then dividing by its standard deviation. Then these standardised reanalysis data of potential predictors were used for the development of the GEP-based downscaling models for each calendar month at each station. For the development of

GEP-based downscaling models, the procedure detailed in section 3.1 was followed.

The mismatch between the outputs of the downscaling model and the corresponding observations is described as the bias in the outputs of a downscaling model (Salvi *et al.,* 2011). Bias in the outputs of a downscaling model is mainly due to the bias in the inputs to the downscaling model (e.g. GCM outputs). In this study, in order to quantify the bias introduced by the GCM to the minimum (or maximum) temperature reproduced by the downscaling model, the twentieth-century climate experiment (20C3M) data of a GCM pertaining to the best potential predictors were standardised using the means and the standard deviations of the corresponding reanalysis outputs of the model calibration period. Then these standardised data were introduced to the best downscaling models identified for each calendar month at each observation station. The minimum (or maximum) temperature reproduced by the downscaling models for the past climate with the 20C3M data of the GCM of interest were numerically compared with observations for the identification of bias in the predictions. Then the bias in the minimum (or maximum) temperature reproduced by the downscaling models for the past climate with the 20C3M data of a GCM were corrected using the monthly bias-correction (MBC) technique for each calendar month. The MBC technique is a relatively simple bias-correction which corrects the bias in the mean and the standard deviation of the variable of interest. More details on the theory and application of the MBC technique can be found in Johnson and Sharma (2012) and Sachindra *et al.* (2014b).

In the application of MBC, first, the minimum (or maximum) temperature reproduced by the downscaling models for the past climate with the 20C3M data of the GCM were standardised with its mean and standard deviation. Then for the correction of bias in the mean and the standard deviation, these standardised data were rescaled using the mean and the standard deviation of observations pertaining to the calibration phase of the downscaling models for each calendar month. For the validation of the effectiveness of the MBC technique, the standardised temperature data produced by the downscaling models pertaining to the model validation phase were rescaled using the mean and the standard deviation of observations relevant to the model calibration phase. This procedure was performed for each calendar month for both rural and urban stations. The performance of the MBC technique was numerically assessed by comparing the statistics of bias-corrected minimum (or maximum) temperature with those of observations in its application and validation periods.

Thereafter the outputs of the GCM pertaining to a future GHG emission scenario (e.g. A2) were standardised with the means and the standard deviations of reanalysis outputs of the calibration period. Then these data were introduced to the downscaling models to project the minimum (or maximum) temperature at the urban and the rural stations into the future. For the application of MBC, these projections produced into the future were again standardised with the means and the standard deviations of temperature reproduced by the downscaling models for the past climate with the 20C3M data of the GCM relevant to the calibration period. Then these standardised data were rescaled with the means and the standard deviations of observations relevant to the calibration period of the model for correcting the bias in each calendar month. The bias-corrected temperature projections produced into the future at the rural and urban stations were applied to Eq. (3) for computing the UHI intensity at the urban station for each calendar month.

3.5. Downscaling models for number of very hot and very cold days

Downscaling models for predicting the number of very hot days in each calendar month in summer and very cold days in each calendar month in winter for the urban city centre were developed following the procedure detailed in section 3.1. The major advantage of direct downscaling of monthly GCM outputs to the number of very hot days and very cold days in calendar months is that it avoids the need for downscaling daily GCM outputs to daily minimum/maximum temperature for the determination of the number of very hot days and very cold days in calendar months. Downscaling daily GCM outputs to daily minimum/maximum temperature needs the management of large sets of input/output data to/from the downscaling models, which is computationally costly.

Initially, temperature thresholds for identifying very hot and cold days were defined. Then considering these thresholds, the number of very hot days in summer and very cold days in winter for each month were counted from the record of daily temperature observations at the urban station. The thresholds for the identification of very hot days in summer and very cold days in winter were defined in such a way that such days occur mainly in summer and winter months.

The same atmospheric domain and the pool of probable predictors used in the development of downscaling models for temperature were also used for development of downscaling models for the number of very hot and very cold days at the urban station. Then using the same procedure used in the development of downscaling models for minimum (or maximum) temperature, GEP-based models for downscaling reanalysis data to number of very hot days in summer and very cold days in winter in each calendar month were developed. In this process, the best downscaling models for each calendar month for downscaling very hot days in summer and very cold days in winter were identified.

Then the 20C3M data of the GCM corresponding to the best potential predictors were standardised with the means and the standard deviations of the reanalysis data pertaining to the calibration phase of the models and used on the best downscaling models to reproduce the observed number of very hot days in summer and very cold days in winter in each calendar month. Then by comparing the observed and model simulated number of very hot days in summer and very cold days in winter in each calendar month, the bias in the downscaled number of very hot days in summer and very cold days in winter was identified. Thereafter, by applying the MBC technique to the time series of very hot days in summer months and very cold days in winter months, the bias in the means and standard deviations of these time series was corrected. For this purpose the same procedure used in correcting the bias in the minimum (or maximum) temperature at the urban and rural stations was employed.

For projection of number of very hot days in summer and very cold days in winter into the future at the urban station, the GCM outputs corresponding to a future GHG emission scenario were standardised with the means and the standard deviations of reanalysis outputs of the model calibration period for each calendar month in summer and winter. Then these standardised GCM outputs corresponding to the future GHG emission scenario were introduced to the best downscaling models identified for each calendar month for projecting the number of very hot days in summer and very cold days in winter into the future. Similar to the application of MBC to the minimum (or maximum) temperature projected into the future at the rural and urban stations, the MBC technique was applied to the time series of the number of very hot and very cold days projected into the future at the urban station for the correction of bias in their means and standard deviations.

4. Application

The generic methodology described in the previous section was applied to weather observation stations located in the CBD of Melbourne and Laverton in Victoria, Australia. The methodology of this study is demonstrated using the outputs of several GCMs (HadCM3, GFDL2.0 and ECHAM5) corresponding to

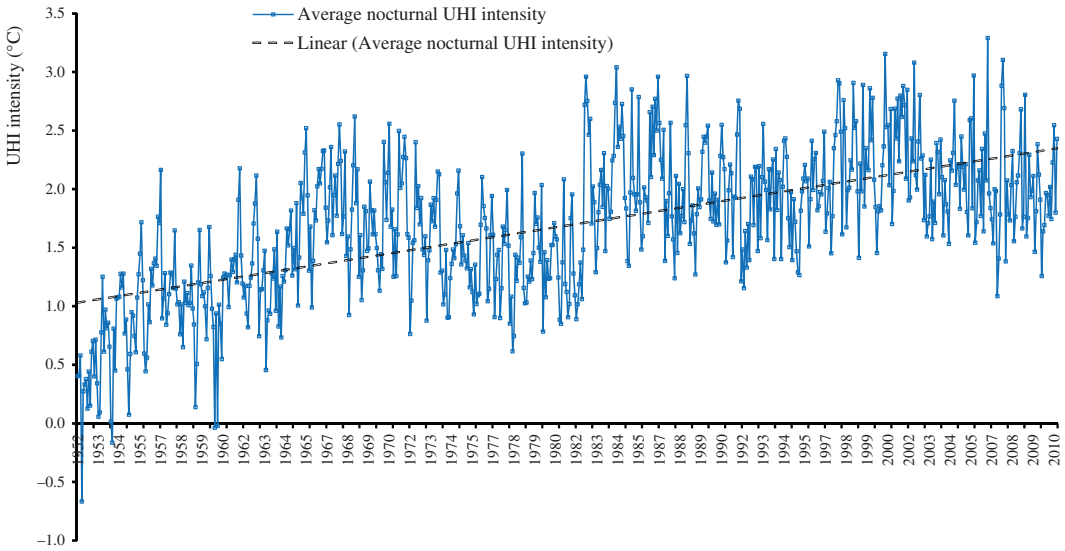

Figure 3. Average monthly nocturnal urban heat island intensity (°C) in CBD of Melbourne, 1952–2010.

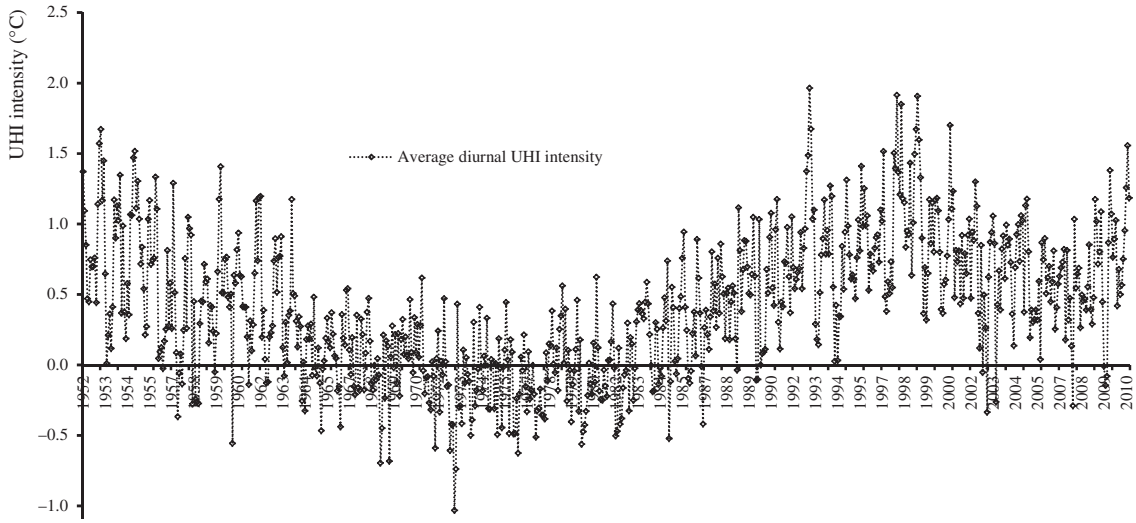

Figure 4. Average monthly diurnal urban heat island intensity (°C) in CBD of Melbourne, 1952–2010.

a greenhouse gas emission scenario (A2). The station located in Melbourne CBD represented the urban environment while the station located in Laverton referred to a less urbanised environment which was assumed to closely represent a rural environment. Ideally, the intensity of a UHI should be computed as the temperature of an urban area with respect to that of a nearby rural area. However, in this study due to the unavailability of a nearby station located in a rural area with a long record of temperature observations, Laverton observation station located in a less urbanized area was selected as the reference station. The intensity of the UHI and the number of very hot days in summer and the number of very cold days in winter in the CBD of Melbourne were projected into the future accounting for likely climate change. It was assumed that the size and the population of the city will remain the same in the future as in the past. Though this assumption seemed to be coarse, it enabled the identification of the impact of climate change on the intensity of Melbourne's UHI.

4.1. *Intensity of urban heat island in the CBD of Melbourne*

The daily nocturnal UHI intensity for the CBD of Melbourne was computed using the daily observations of minimum temperatures at Melbourne and Laverton and hence the average monthly nocturnal UHI intensity for the CBD of Melbourne was derived. Similarly, using the daily observations of maximum temperatures at Melbourne and Laverton the average monthly diurnal UHI intensity for the CBD of Melbourne was computed.

The computation of nocturnal and diurnal UHI intensities at the CBD of Melbourne was performed using Eq. (3). Figures 3 and 4 show the average monthly nocturnal and diurnal UHI intensities over the period 1952–2010 in the CBD of Melbourne, respectively.

According to Figure 3, it was seen that the nocturnal UHI intensity is more consistently higher than the diurnal UHI in the CBD of Melbourne. Furthermore, the nocturnal UHI intensity in Melbourne CBD displayed a clear rising trend (refer to the linear trend line in Figure 3) over the period 1952–2010, unlike the diurnal UHI intensity. Owing to the clear rising trend, in this study, the investigation was confined to the nocturnal UHI intensity. During the night-time, urban structures such as concrete buildings which have high thermal capacities tend to slowly release heat energy that they absorbed during the daytime. This causes the air in the urban environment to cool less in comparison to that of surrounding rural settings during night-time.

4.2. *Atmospheric domain and predictor selection*

An atmospheric domain with 3×3 grid points at a spatial resolution of 2.5° has been successfully used by Anandhi *et al.* (2009, 2012) for downscaling GCM outputs to monthly average minimum and maximum temperature and also to daily

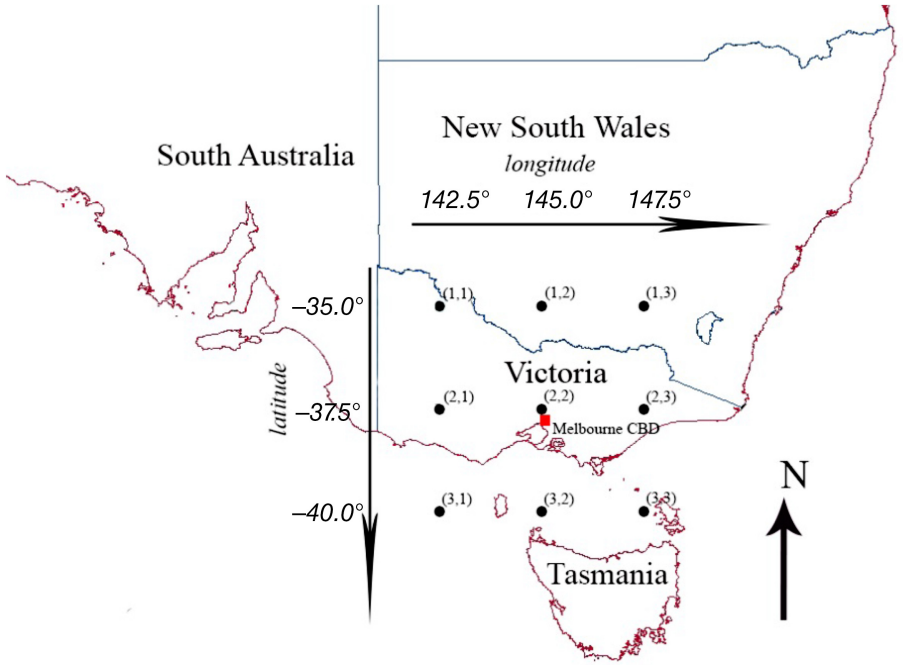

Figure 5. Atmospheric domain for the downscaling models.

evaporation. Therefore, in this study, an atmospheric domain with spatial dimensions of 3 × 3 grid points at a spatial resolution of 2.5° in both longitudinal and latitudinal directions was selected. The size of this atmospheric domain was determined considering its ability to represent the large-scale atmospheric phenomena which influence the temperature at the points of interest and also the computational cost. The atmospheric domain used in this study is shown in Figure 5.

A set of probable predictors for the downscaling models for monthly minimum temperature and the number of very hot and very cold days was selected based on the studies by Anandhi *et al.* (2008) and Timbal *et al.* (2009). Timbal *et al.* (2009) identified a set of predictor variables influential on the minimum and maximum temperature, over south and southeastern Australia which includes the present study area.

The set of probable predictors used in the current study for the downscaling models included: geopotential heights at 200, 500, 700, 850 and 1000 hPa pressure levels; relative humidity at 500, 700, 850 and 1000 hPa pressure levels; specific humidity at 2 m height, 500, 850 and 1000 hPa pressure levels; air temperature at surface, 2 m height, 500, 850 and 1000 hPa pressure levels; surface skin temperature; surface pressure; mean-sea-level pressure; surface precipitation rate; and precipitable water content.

The monthly data for these 23 probable predictors for the nine grid points shown in Figure 5 were obtained from the NCEP/NCAR reanalysis data archive at http://www.esrl.noaa.gov/psd/ for the period 1952–2010. Then the correlation coefficients between observed monthly minimum temperature and the NCEP/NCAR reanalysis data for each of the probable predictors were computed for the period 1952–2010 for each calendar month. As described in the generic methodology, the probable predictors which were statistically significant at the 95% confidence level ($p = 0.05$) were selected as the potential predictors for each calendar month for the development of downscaling models for monthly minimum temperature. The above procedure was practised for each calendar month for the stations at Melbourne CBD and Laverton separately.

4.3. Downscaling models for monthly minimum temperature at Melbourne and Laverton

In order to develop downscaling models for monthly minimum temperature, the observed monthly minimum temperature at Melbourne and Laverton, and NCEP/NCAR reanalysis data for potential predictors, were split into two chronological groups: (i) 1952–1989 for calibration and (ii) 1990–2010 for validation. The software package called 'GeneXproTools' was used for building the gene expression programming (GEP) based downscaling models. In developing GEP-based downscaling models, addition, subtraction, multiplication, division, exponential, natural logarithm, inverse, power of 2, power of 3, cube root, sine, cosine and arctangent were selected as the mathematical functions, and as genetic operators, replication, mutation, transposition and recombination (cross-over) were selected. Though 'GeneXproTools' offers a large variety of functions, the set of functions selected in this study was limited to the above 13, as large number of functions can produce over-complex downscaling models which can cause over-fitting in calibration and under-fitting in validation. Hashmi *et al.* (2011) also successfully used the same set of functions and genetic operators for developing a precipitation downscaling model.

Thereafter, the ten probable predictors which showed the highest statistically significant ($p = 0.05$) correlations with observed monthly minimum temperature over the period 1952–2010 were selected for each calendar month, for Melbourne and Laverton separately. Then the NCEP/NCAR reanalysis data pertaining to these ten probable predictors for the period 1952–2010 were standardised with their means and standard deviations of the period 1952–1989. Initially, 30 GEP-based downscaling models were randomly generated for each calendar month (initial population) for each station. Then following the procedure detailed in the generic methodology, for the period 1952–1989, GEP-based downscaling models were evolved up to 10 000 generations by performing the previously stated genetic operations. In each generation the number of downscaling models was maintained at 30 for each calendar month. In GEP-based modelling, evolution of a model is analogous to model calibration.

Then each of these models was validated using the observed monthly minimum temperature and the standardised NCEP/NCAR reanalysis data pertaining to the ten probable predictors for the period 1990–2010. In each generation the goodness of fit of each model was measured using the RMSE. With the evolution of downscaling models, over-fitting in calibration and under-fitting in validation was observed. Therefore, the model which showed the best performance in terms of the RMSE (lowest RMSE) in validation was selected as the best model for a calendar month. In the above manner statistical downscaling

Table 1. Statistics of observed and modelled minimum temperature in Melbourne and Laverton.

Statistic	Melbourne CBD				Laverton			
	Calibration (1952–1989)		Validation (1990–2010)		Calibration (1952–1989)		Validation (1990–2010)	
	Obs	Model with NCEP/NCAR	Obs	Model with NCEP/NCAR	Obs	Model with NCEP/NCAR	Obs	Model with NCEP/NCAR
Avg	10.7	10.9	11.6	11.3	9.2	9.3	9.5	9.4
Std	3.2	3.2	3.2	3.3	3.3	3.3	3.3	3.3
C_v	0.30	0.29	0.28	0.29	0.36	0.35	0.35	0.35
NSE		0.96		0.95		0.96		0.95
R^2		0.96		0.96		0.96		0.95

Avg = average of monthly minimum temperature in °C, Std = standard deviation of monthly minimum temperature in °C, C_v = coefficient of variation of minimum monthly temperature, NSE = Nash–Sutcliffe efficiency, R^2 = coefficient of determination, Obs = derived from observations.

models were developed for Melbourne and Laverton for each calendar month.

Table 1 shows the statistics of the observed and modelled monthly minimum temperature in the CBD of Melbourne and Laverton. According to Table 1, it was realised that in both calibration and validation, the average, the standard deviation and the coefficient of variation of the monthly minimum temperature in the CBD of Melbourne and Laverton are reproduced with a high degree of accuracy by the model. Therefore it was realised that the downscaling models developed for Melbourne and Laverton were capable in mimicking the statistics of observed monthly minimum temperature in Melbourne and Laverton with NCEP/NCAR reanalysis outputs.

Figure 6 shows the scatter plots for the downscaling models for monthly minimum temperature at Melbourne and Laverton. Figure 6(a, b) refer to the calibration and validation phases of the downscaling model for monthly minimum temperature at Melbourne respectively, while Figure 6(c, d) refer to Laverton. According to Figure 6, it was realised that the monthly minimum temperature predicted by downscaling models at Melbourne and Laverton are in very good agreement with corresponding observations, both in the calibration and validation periods.

Table 2 shows the statistics of nocturnal UHI intensities in the CBD of Melbourne derived from observed and modelled (using downscaling models with NCEP/NCAR reanalysis data) monthly minimum temperature in the CBD of Melbourne and Laverton, over the period 1952–2010. As shown in Table 2, it was clear that the averages and the standard deviations of UHI intensity derived from the observed minimum temperature and the minimum temperature reproduced by the downscaling models are in very good agreement with each other for the majority of the calendar months. The maximum of UHI intensity computed from the monthly minimum temperature reproduced by the downscaling models was slightly overestimated in comparison to the UHI intensity derived from the observations, in the majority of the calendar months.

4.3.1. Bias-correction of monthly minimum temperature at Melbourne and Laverton

As shown in the previous section, statistics of the monthly minimum temperature reproduced by downscaling models run with the NCEP/NCAR reanalysis outputs were in good agreement with the corresponding statistics derived from observed monthly minimum temperature at both stations. However, when these downscaling models are run with outputs of HadCM3, GFDL2.0 and ECHAM5, a mismatch between the statistics of the model-simulated minimum temperature and statistics of observed minimum temperature is expected. This is because unlike the NCEP/NCAR reanalysis outputs which are quality controlled and corrected against observations, outputs of HadCM3, GFDL2.0 and ECHAM5 are not subject to such corrective or quality-control measures. Therefore, there is a need to quantify the bias (mismatch) in the monthly minimum temperature produced by the downscaling models when run with outputs of HadCM3, GFDL2.0 and ECHAM5 and subsequently the bias should be corrected.

For the quantification and correction of bias in the monthly minimum temperature, the 20C3M data of HadCM3, GFDL2.0 and ECHAM5 for the period 1952–1999 were standardised with the means and the standard deviations of corresponding NCEP/NCAR reanalysis outputs of the period 1952–1989. The 20C3M data of the GCMs refer to the climate of the past century and they are analogous to the NCEP/NCAR reanalysis outputs of the past century. Therefore, a comparison between monthly minimum temperatures downscaled using the 20C3M data of GCMs and NCEP/NCAR reanalysis outputs enables the quantification bias introduced to monthly minimum temperature by the GCMs. Then the standardised 20C3M data of HadCM3, GFDL2.0 and ECHAM5 were introduced to the best downscaling models developed for each calendar month, for reproducing the observations of monthly minimum temperature of the period 1952–1999, at the stations in the Melbourne CBD and Laverton. The monthly bias-correction (MBC) was then applied to the individual time series of monthly minimum temperature reproduced by the downscaling models run with the 20C3M outputs of HadCM3, GFDL2.0 and ECHAM5 for the period 1952–1989 and it was validated over the period 1990–1999. The procedure for the application and validation of MBC is detailed in the generic methodology. Table 3 shows the statistics of observed monthly minimum temperature and those of monthly minimum temperature reproduced by the downscaling models when run with the 20C3M data of HadCM3, GFDL2.0 and ECHAM5 for the periods 1952–1989 and 1990–1999, before and after the application of bias-correction.

As shown in Table 3, it was clear that at Melbourne and Laverton, when the downscaling models were run with the 20C3M data of HadCM3, GFDL2.0 and ECHAM5 (before bias-correction), the average and the minimum of monthly minimum temperature were underestimated and the standard deviation was overestimated in both application and validation periods of the bias-correction. However, after the application of the MBC technique, during both application (1952–1989) and validation (1990–2010) periods, the bias in the statistics of the monthly minimum temperature reproduced by the downscaling models run with outputs of HadCM3, GFDL2.0 and ECHAM5 at Melbourne and Laverton reduced quite largely. This indicated that the MBC technique is effective in reducing the bias in the statistics of monthly minimum temperature.

4.3.2. Projection of monthly minimum temperature at Melbourne and Laverton, and hence UHI intensity in the CBD of Melbourne

The outputs of HadCM3, GFDL2.0 and ECHAM5 for the A2 GHG emission scenario pertaining to the potential predictors used in developing the downscaling models were obtained for the period 2000–2099. Then these data were standardised with the means and the standard deviations of NCEP/NCAR reanalysis data of the period 1952–1989. Thereafter the standardised outputs of HadCM3, GFDL2.0 and ECHAM5 for the A2 GHG

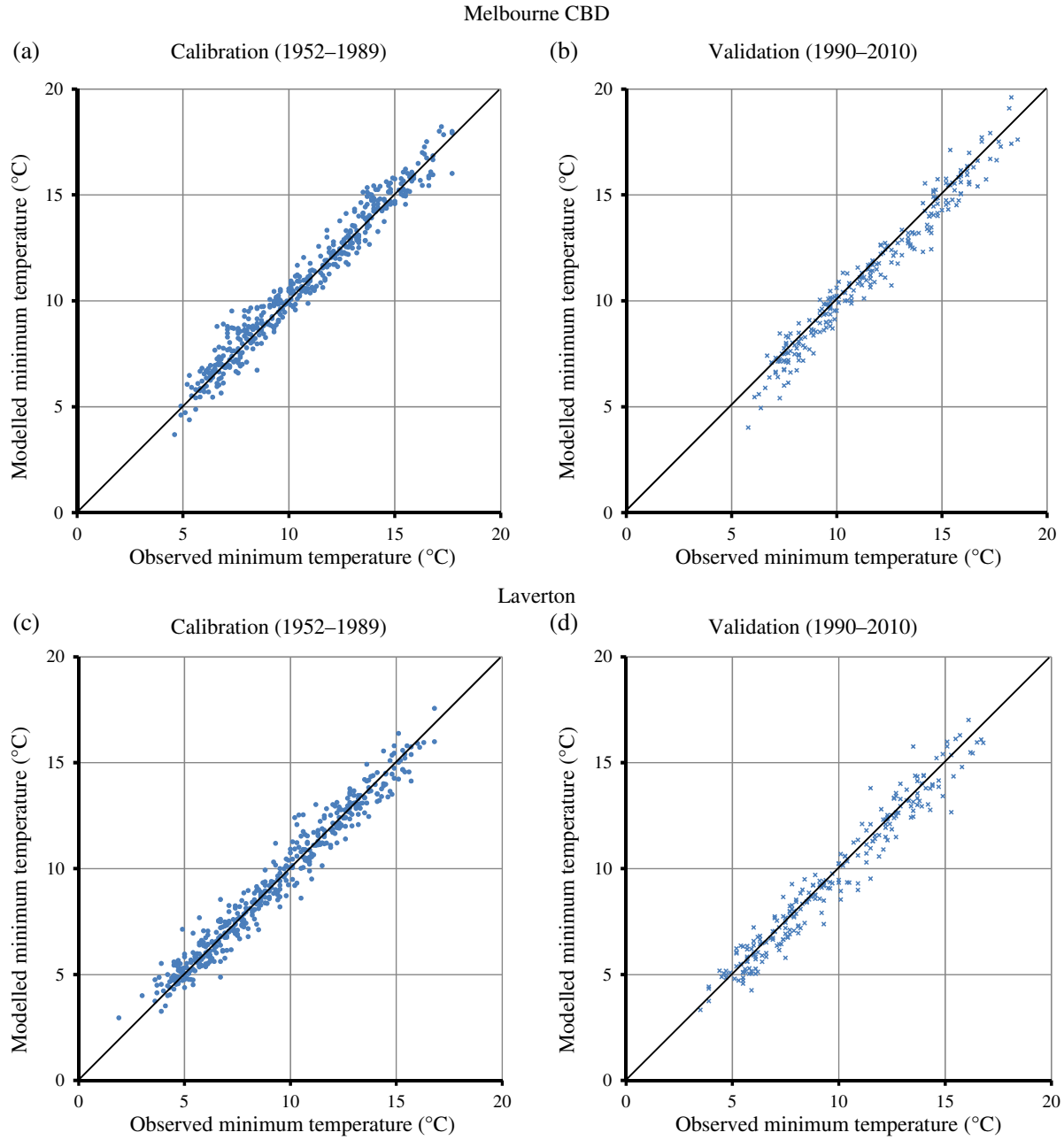

Figure 6. Scatter plots for the downscaling models for monthly minimum temperature (°C) at (a, b) Melbourne and (c, d) Laverton, with (a, c) calibration (1952–1989) and (b, d) validation (1990–2010).

Table 2. Statistics of nocturnal urban heat island intensities at CBD of Melbourne, derived from observed and modelled monthly minimum temperature (1952–2010).

Month	Average		Standard deviation		Minimum		Maximum	
	Obs	Modelled	Obs	Modelled	Obs	Modelled	Obs	Modelled
January	1.5	1.4	0.6	0.9	0.0	0.4	2.8	4.0
February	1.4	1.9	0.6	0.6	−0.1	0.6	2.8	3.5
March	1.5	1.8	0.6	0.6	0.4	−1.2	2.7	4.2
April	1.6	1.4	0.7	0.8	−0.8	−0.4	2.9	3.3
May	1.6	1.6	0.6	0.8	0.1	−0.5	3.1	3.2
June	1.6	1.4	0.5	0.5	0.4	−0.2	3.0	2.3
July	1.7	1.6	0.5	0.6	0.4	0.4	2.8	3.1
August	1.8	1.7	0.6	0.7	0.1	−0.5	3.1	3.2
September	2.0	2.5	0.6	0.6	0.4	0.8	3.1	4.0
October	2.0	2.1	0.6	0.7	0.3	0.6	3.3	4.3
November	1.8	1.6	0.5	0.9	0.6	−0.1	2.9	3.3
December	1.7	1.6	0.5	0.7	0.7	0.3	3.0	3.2

Obs = derived from observations at Melbourne CBD and Laverton (°C), Modelled = derived from the minimum temperature reproduced by downscaling models at Melbourne CBD and Laverton (°C).

Table 3. Statistics of monthly minimum temperature derived from observations and model runs with 20C3M data of HadCM3, GFDL2.0 and ECHAM5 before and after bias-correction.

	Melbourne						Laverton					
Statistic	Obs (1952–1989)	Application (1952–1989)		Obs (1990–1999)	Validation (1990–1999)		Obs (1952–1989)	Application (1952–1989)		Obs (1990–1999)	Validation (1990–1999)	
		Before bias-correction	*After bias-correction*		*Before bias-correction*	*After bias-correction*		*Before bias-correction*	*After bias-correction*		*Before bias-correction*	*After bias-correction*
Avg	**10.7**	9.3/9.6/*8.8*	10.7/10.7/*10.7*	**11.3**	9.4/9.3/*9.1*	11.0/10.9/*11.1*	**9.2**	9.0/9.1/*9.0*	9.2/9.2/*9.2*	**9.2**	9.0/9.1/*8.9*	9.2/9.2/*9.1*
Std	**3.2**	6.8/6.9/*6.1*	3.2/3.2/*3.2*	**3.1**	7.2/6.9/*6.0*	3.4/3.3/*3.4*	**3.3**	3.8/3.4/*3.6*	3.3/3.3/*3.3*	**3.2**	4.0/4.1/*3.8*	3.5/3.9/*3.5*
C_v	**0.30**	0.73/0.72/*0.69*	0.30/0.30/*0.30*	**0.28**	0.76/0.74/*0.66*	0.31/0.30/*0.31*	**0.36**	0.42/0.37/*0.40*	0.36/0.36/*0.36*	**0.35**	0.44/0.45/*0.43*	0.38/0.42/*0.38*
Min	**4.6**	−16.5/−19.8/*−8.6*	5.0/4.1/*6.2*	**5.8**	−16.4/−16.0/*−11.2*	5.0/4.7/*5.6*	**1.9**	0.7/0.9/*0.2*	2.1/2.2/*2.0*	**3.5**	0.2/0.6/*−1.2*	3.4/3.5/*3.0*

Avg = average of monthly minimum temperature in °C, Std = standard deviation of monthly minimum temperature in °C, C_v = Coefficient of variation of minimum monthly temperature, Min = minimum of monthly minimum temperature in °C, Obs = derived from observations, Bold text refer to statistics of monthly minimum temperature derived from observations, Plain text refer to statistics of monthly minimum temperature reproduced by downscaling model run with HadCM3, Underlined text refer to statistics of monthly minimum temperature reproduced by downscaling model run with GFDL2.0, Italicised text refer to statistics of monthly minimum temperature reproduced by downscaling model run with ECHAM5.

Table 4. Statistics of observed monthly minimum temperature for past period 1952–2010 and projected ensemble monthly minimum temperature for future period 2000–2099.

Scenario	Time slice	Statistic	Melbourne				Laverton			
			Summer	Autumn	Winter	Spring	Summer	Autumn	Winter	Spring
Observations	1952–1971	Avg	14.2	11.0	6.7	9.5	13.1	10.0	5.3	7.9
		Std	1.5	2.3	0.9	1.6	1.6	2.3	1.0	1.6
	1972–1991	Avg	14.8	12.0	7.3	10.6	13.3	10.3	5.5	8.6
		Std	1.3	2.1	1.0	1.5	1.6	2.3	1.1	1.7
	1992–2010	Avg	15.5	12.1	7.8	10.9	13.6	10.1	5.7	8.6
		Std	1.5	2.2	0.8	1.7	1.7	2.2	1.0	1.9
A2 GHG emission scenario	2000–2019	Avg	*15.2**	*12.8**	*8.3**	*9.4*	*13.2*	*10.1*	*5.3*	*8.3**
		Std	*1.6*	*1.7**	*2.2**	*1.8*	*1.5*	*2.2*	*1.1*	*1.9*
	2020–2039	Avg	*16.5**	*13.1**	*8.8**	*10.3**	*13.5*	*11.1**	*5.5*	*8.8**
		Std	*2.2**	*2.7**	*1.9**	*1.9*	*1.4*	*3.0**	*1.4*	*2.3**
	2040–2059	Avg	*17.4**	*14.3**	*9.1**	*10.6**	*14.1**	*12.1**	*5.9**	*9.2**
		Std	*2.6**	*4.0**	*1.8**	*2.1**	*1.8*	*3.3**	*1.7**	*2.5**
	2060–2079	Avg	*18.4**	*15.2**	*9.5**	*11.4**	*14.9**	*13.5**	*6.3**	*9.6**
		Std	*2.5**	*4.2**	*1.5**	*2.9**	*3.0**	*4.8**	*2.1**	*2.9**
	2080–2099	Avg	*19.6**	*15.6**	*9.8**	*11.5**	*16.3**	*14.5**	*7.2**	*10.2**
		Std	*2.7**	*4.5**	*1.5**	*3.3**	*4.0**	*5.3**	*1.9**	*3.3**

Avg = average of monthly minimum temperature in °C, Std = standard deviation of monthly minimum temperature in °C, Min = minimum of monthly minimum temperature in °C, * = statistically significant change ($p = 0.05$) in mean/standard deviation with respect to that in period 1952–1971.

emission scenario were introduced to the downscaling models for the projection of monthly minimum temperature into the future period 2000–2099, in Melbourne CBD and Laverton. The bias in the means and the standard deviations of these projections of monthly minimum temperature was corrected using the MBC technique. Then the ensemble average monthly minimum temperature time series for each calendar month was computed by adding the individual time series of monthly minimum temperature projected using the outputs of HadCM3, GFDL2.0 and ECHAM5 for the A2 GHG emission scenario and averaging them (e.g. Sachindra *et al.*, 2014d). Table 4 shows the statistics of observed monthly minimum temperature for the past period 1952–2010 and projected ensemble average monthly minimum temperature under the A2 GHG emission scenario for the future period 2000–2099 at Melbourne and Laverton. The statistics derived from observed monthly minimum temperature are shown under three 20-year time slices: 1952–1971, 1972–1991 and 1992–2010. The statistics derived from monthly minimum temperature projected into the future are shown under five 20-year time slices: 2000–2019, 2020–2039, 2040–2059, 2060–2079 and 2080–2099. According to Table 4, during the period 1952–2010, the average of the observed monthly minimum temperature at both Melbourne and Laverton stations showed an increasing trend in all seasons. In this study, seasons are defined as summer (December–February), autumn (March–May), winter (June–August) and spring (September–November). As shown in Table 4, the two-sample *t*-test revealed that the increase in the average of monthly minimum temperature at the CBD of Melbourne and Laverton in all seasons in the time slices 2040–2059, 2060–2079 and 2080–2099 are significant at the 95% confidence level with respect to the average of monthly minimum temperature in the period 1952–1972. The period 1952–1972 was selected as the baseline since the changes in the climate during that period was minimum. Also, the two-sample *F*-test indicated that the rise in the standard deviation of monthly minimum temperature at the CBD of Melbourne and Laverton projected into the future compared to that of monthly minimum temperature for the period 1952–1971 was statistically significant at the 95% confidence level in all seasons in the time slices 2060–2079 and 2080–2099. This indicated that with the rising GHG concentrations in the atmosphere the monthly minimum temperature at both urban and rural stations tends to increase and also it will have more fluctuations.

Table 5 shows the statistics of nocturnal UHI intensity at the CBD of Melbourne computed based on the observed monthly minimum temperature for the past period 1952–2010 and the projected monthly minimum temperature for the future period 2000–2099. In Table 5, it was seen that the average, the minimum and the maximum of the nocturnal UHI intensity (computed with observed minimum temperature) at the CBD of Melbourne showed a rising trend in the three time slices 1952–1971, 1972–1991 and 1992–2010, in all four seasons. However, the standard deviation of the UHI intensity remained almost stationary throughout the above three time slices in all four seasons.

As shown in Table 5, under the A2 GHG emission scenario, the two-sample *t*-test indicated that the increase in the average of nocturnal UHI intensity at the CBD of Melbourne in summer, winter and spring in the time slices 2020–2039, 2040–2059 and 2060–2079 are significant at the 95% confidence level with respect to the nocturnal UHI intensity in the period 1952–1972.

Table 5. Statistics of nocturnal urban heat island intensity at CBD of Melbourne (derived from ensemble temperature projections).

Scenario	Time slice	Statistic	Summer	Autumn	Winter	Spring
Observations	1952–1971	Avg	**1.1**	**1.1**	**1.4**	**1.6**
		Std	**0.5**	**0.6**	**0.5**	**0.6**
	1972–1991	Avg	**1.5**	**1.6**	**1.8**	**2.0**
		Std	**0.5**	**0.5**	**0.5**	**0.5**
	1992–2010	Avg	**1.9**	**2.0**	**2.1**	**2.3**
		Std	**0.4**	**0.4**	**0.4**	**0.4**
A2 GHG emission scenario	2000–2019	Avg	*1.4*	*2.3**	*3.0**	*1.6*
		Std	*1.1**	*2.5**	*1.8**	*1.7**
	2020–2039	Avg	*1.9**	*1.6*	*3.4**	*2.0**
		Std	*1.4**	*4.3**	*1.7**	*1.5**
	2040–2059	Avg	*2.1**	*1.9*	*3.3**	*1.9**
		Std	*2.0**	*6.4**	*1.4**	*1.7**
	2060–2079	Avg	*2.4**	*1.3*	*3.2**	*2.2**
		Std	*2.7**	*7.9**	*1.8**	*2.3**
	2080–2099	Avg	*2.2**	*0.6*	*2.7**	*1.7*
		Std	*3.2**	*9.0**	*1.8**	*1.8**

Avg = average of monthly UHI intensity in °C, Std = standard deviation of monthly UHI intensity in °C, Min = minimum of monthly UHI intensity in °C, Max = maximum of monthly UHI intensity in °C, Bold text refers to statistics of UHI intensity derived from observations of average monthly minimum temperature, Italicised text refers to statistics of UHI intensity derived from ensemble average monthly minimum temperature time series, * = statistically significant change ($p = 0.05$) in the statistic with respect to that in period 1952–1971.

Furthermore, the two-sample *F*-test showed that the rise in the standard deviation of nocturnal UHI intensity at the CBD of Melbourne projected into the future compared to that of nocturnal UHI intensity of period 1952–1971 was statistically significant at the 95% confidence level in all seasons throughout the twenty-first century. It should be noted that in this study the future expansion of the city and its population have not been accounted for in the models. The future expansion of the city and its population can further increase the effect of the UHI in the CBD of Melbourne.

4.4. Downscaling models for number of very hot and very cold days in the CBD of Melbourne

Similar to the development of the downscaling models for monthly minimum temperature, models for downscaling NCEP/NCAR reanalysis outputs to the number of very hot and very cold days in the CBD of Melbourne were developed. For this purpose, the same pool of probable predictors used for downscaling temperature was considered. Then for each calendar month in summer (December–February) and winter (June–August) and also one month before and after these seasons (ten calendar months), potential predictors were extracted from this pool of probable predictors, as described in the generic methodology. Summer and winter months were selected as they are the months which have the highest number of very hot and very cold days, respectively. In other words, most of the extreme temperature events occur during the summer and winter months.

In this study, a very hot day was defined as a day with maximum temperature exceeding 35 °C and a very cold day was defined as a day on which the minimum temperature drops below 5 °C. Then for each calendar month in summer and one month before (November) and after (March) summer, the number of very hot days (temperature above 35 °C) was counted from the observed records of daily maximum temperature at the CBD of Melbourne for the period 1952–2010. The months before and after summer were also considered in this study as these months still encompass days with maximum temperature exceeding 35 °C. Also in the future, the changes in the number of days with maximum temperature exceeding 35 °C under changing climate in the months which precede and follow summer can indicate possible changes in the beginning and end of summer. Similarly, for each calendar month in winter and one month before (May) and after (September) winter, the number of very cold days (temperature below 5 °C) was counted from the observed records of daily minimum temperature at the CBD of Melbourne for the period 1952–2010. The months before and after winter were also considered in this study as these months still encompass days with minimum temperature lower than 5 °C. Also in the future, the changes in the number of days with minimum temperature below 5 °C under changing climate in the months which precede and follow winter can indicate the possible changes in the beginning and end of winter. Using the number of very hot (November–March) and very cold (May–September) days for each calendar month as the predictand, statistical downscaling models were developed for the station at the Melbourne CBD for each calendar month.

Table 6 shows the results of the calibration and validation of the downscaling models for the number of very hot days and very cold days in the CBD of Melbourne. According to Table 6, it was seen that the downscaling model was able to reproduce the average, the standard deviation, the minimum and the maximum of the number of very hot days in summer months with a good degree of accuracy in both calibration and validation periods with NCEP/NCAR reanalysis outputs. Also, the downscaling model was able to reproduce the average number of very cold days in the winter months with good accuracy. However, the standard deviation of the number of very cold days was not properly simulated particularly in July. Also in both calibration and validation periods, the minimum and the maximum number of very cold days in a month was not correctly predicted by the downscaling model. Therefore, it was understood that this model was more reliable in predicting the average number of very cold days in winter months, rather than the other statistics of the number of very cold days in winter months.

Similar to the downscaling model for monthly minimum temperature, the downscaling models for the number of very hot and very cold days were run with the 20C3M outputs of HadCM3, GFDL2.0 and ECHAM5 and the MBC technique was applied to the number of very hot and very cold days predicted by the models during the period 1952–1989. The intention of this step was to identify the bias in the number of very hot and very cold days simulated by the downscaling models when they were run with 20C3M outputs of HadCM3, GFDL2.0 and ECHAM5, and its subsequent correction. The performance of the MBC technique in correcting the bias in the number of very hot and very cold days was validated over the period 1990–1999. It was seen that MBC was effective in correcting the bias in the statistics of the number of very hot and very cold days reproduced by the downscaling model run with the 20C3M outputs of HadCM3, GFDL2.0 and ECHAM5 in the application and validation periods (results not shown).

Table 6. Calibration and validation of downscaling models for number of very hot days and very cold days in CBD of Melbourne.

Phase	Time slice	Statistic	November	December	January	February	March	May	June	July	August	September
			Very hot days ($T_{max} > 35°C$)					Very cold days ($T_{min} < 5°C$)				
			O(M)	O(M)	O(M)	O(M)	O(M)	O(M)	O(M)	O(M)	O(M)	O(M)
Calibration	1952–1989	Avg	1(1)	2(2)	4(4)	2(2)	1(1)	*2 (2)*	*6(6)*	*9(8)*	*5(5)*	*3(3)*
		Std	1(1)	2(2)	3(2)	2(2)	1(1)	*2(1)*	*4(3)*	*4(0)*	*3(2)*	*2(2)*
		Min	0(0)	0(0)	0(0)	0(0)	0(0)	*0(1)*	*1(0)*	*1(8)*	*0(3)*	*0(0)*
		Max	4(3)	7(7)	11(9)	9(8)	4(3)	*7(6)*	*18(18)*	*17(8)*	*13(12)*	*9(7)*
Validation	1990–2010	Avg	0(1)	2(2)	4(3)	3(2)	1(1)	*2(2)*	*4(5)*	*5(8)*	*4(6)*	*3(3)*
		Std	1(1)	2(2)	2(2)	2(2)	1(0)	*1(0)*	*2(2)*	*4(0)*	*3(1)*	*2(2)*
		Min	0(0)	0(0)	1(0)	0(0)	0(0)	*1(1)*	*1(0)*	*0(8)*	*0(4)*	*0(0)*
		Max	2(3)	5(6)	5(7)	7(7)	3(1)	*3(2)*	*6(7)*	*12(8)*	*9(8)*	*7(6)*

Avg = average number of days in a month with maximum (*minimum*) temperature exceeding (*below*) 35 °C (*5* °C), Std = standard deviation of number of days in a month with maximum (*minimum*) temperature exceeding (*below*) 35 °C (*5* °C), Min = minimum number of days in a month with maximum (*minimum*) temperature exceeding (*below*) 35 °C (*5* °C), Max = maximum number of days in a month with maximum (*minimum*) temperature exceeding (*below*) 35 °C (*5* °C), O = derived from observations, M = derived from outputs of downscaling models.

Table 7. Average number of very hot and very cold days in CBD of Melbourne.

Scenario	Time slice	November	December	January	February	March	May	June	July	August	September
		Very hot days ($T_{max} > 35$ °C)					Very cold days ($T_{min} < 5$ °C)				
Observations	1952–1971	**0**	**2**	**4**	**2**	**1**	*3*	*6*	*9*	*7*	*4*
	1972–1991	**1**	**2**	**3**	**2**	**1**	*1*	*6*	*7*	*4*	*2*
	1992–2010	**1**	**2**	**4**	**3**	**1**	*1*	*4*	*5*	*4*	*2*
Ensemble projections	2000–2019	**1**	**3**	**4**	**3**	**0**	*1**	*2**	*1**	*3**	*3*
based on A2 GHG	2020–2039	**1**	**4***	**5**	**5***	**1**	*0**	*1**	*2**	*2**	*6**
emission scenario	2040–2059	**1**	**5***	**6***	**8***	**2***	*0**	*0**	*4**	*7*	*7**
	2060–2079	**1**	**7***	**7***	**11***	**3***	*0**	*0**	*6**	*3**	*10**
	2080–2099	**1**	**9***	**9***	**15***	**4***	*0**	*2**	*12**	*7*	*12**

Bold text refer to average number of very hot days ($T_{max} > 35$ °C) in Melbourne CBD, Italicised text refer to average number of very cold days ($T_{min} < 5$ °C) in Melbourne CBD, * = statistically significant change ($p = 0.05$) in the average number of very hot/cold days with respect to that in period 1952–1971.

For projection of the number of very hot and very cold days into the future at the CBD of Melbourne, the HadCM3, GFDL2.0 and ECHAM5 A2 outputs pertaining to the potential predictors used for developing the downscaling models for number of very hot and very cold days were obtained for the period 2000–2099. These HadCM3, GFDL2.0 and ECHAM5 outputs were standardised using the means and the standard deviations of corresponding NCEP/NCAR reanalysis outputs of the period 1952–1989. Then using the above standardised HadCM3, GFDL2.0 and ECHAM5 outputs corresponding to the A2 GHG emission scenario on the downscaling models, the number of very hot and very cold days in each calendar month in summer and winter were projected into the future period 2000–2099. The bias in the statistics of number of very hot and very cold days in each calendar month in summer and winter were corrected using the MBC technique. Then the ensemble average number of very hot and very cold days in each calendar month in summer and winter were computed using the above bias-corrected time series.

The ensemble average number of very hot and very cold days in summer and winter in the past and in the future (after bias-correction) in the CBD of Melbourne are shown in Table 7.

According to Table 7, the two-sample *t*-test revealed that the average number of very hot days in December, January, February and March shows a statistically significant increase (at 95% confidence level) in the time slices 2040–2059, 2060–2079 and 2080–2099 with respect to the average number of very hot days in the same months in the period 1952–1971. In the past records of observations, such a rise in the average number of very hot days over the three time slices 1952–1971, 1972–1991 and 1992–2010 was not well pronounced. Furthermore, in the past, the highest number of very hot days was recorded in the month of January in all the three time slices. However, a change in this trend was seen after the future time slice 2020–2039, as the average number of very hot days in February was higher than that of January. This was a possible indication that the highest number of very hot days will occur in February during the period 2040–2099 and continue into the future. Also in March, the average number of very hot days showed an increasing trend starting from time slice 2020–2039. This is a possible indication of an expansion of the future summer weather into early autumn in the CBD of Melbourne.

Also as shown in Table 7, the two-sample *t*-test indicated that in May, June, July and August the average number of very cold days displays a statistically significant (at 95% confidence level) decrease in the majority of the time slices in the future. However, in September there is a statistically significant (at 95% confidence level) increase in the average number of very cold days from 2020 onwards. Details in Table 7 lead to the conclusion that, with the rising GHG concentrations in the atmosphere, the autumn weather will move to early winter and winter weather will move to early spring in the CBD of Melbourne. Overall, this study indicated that the number of very hot days will increase and very cold days will decrease with the rising GHG concentrations and hence the thermal comfort in the Melbourne CBD will be affected. Therefore, high cooling loads on buildings are expected with high cost of energy in the CBD of Melbourne in the future.

4.5. *Uncertainties and limitations of the study*

It should be noted that the projections of temperature and number of very hot and very cold days produced in this study using statistical downscaling models are subject to a cascade of uncertainties originating from many sources. These sources include: GHG emission scenarios, GCMs, the downscaling technique used, predictor–predictand stationarity assumption (Sachindra *et al.*, 2014c). The actual amounts of GHG emissions in the future world are unknown. Therefore, a number of equally likely but different GHG emission scenarios is used to represent the levels of GHG emissions corresponding to the future. In this study, the projections of temperature and number of very hot and very cold days were produced corresponding to the A2 GHG emission scenario which is only one of the many GHG emission scenarios in use. Therefore, the projections produced in

this study should be treated as plausible rather than definite. The use of a number of different GHG emission scenarios enables the quantification of impacts of different levels of GHG emissions on the predictand of interest.

Also the projections of a downscaling model vary with the GCM used to produce inputs to that downscaling model. This is because owing to different approximations and assumptions employed in the structures of different GCMs, their projections tend to vary from one another. In the present study, outputs of HadCM3, GFDL2.0 and ECHAM5 were used to produce inputs to the downscaling models. The combination of ensemble of projections using an ensemble modelling technique such as averaging (used in the present study) can reduce the dependence of projections on one specific GCM. Furthermore, using sets of outputs from different GCMs on the downscaling models and deriving an ensemble of projections can better explain the uncertainties (e.g. visualize the upper and lower uncertainty bounds of the predictand) introduced by different GCMs to the projections of the predictand of interest.

The downscaling technique used also can introduce some uncertainties to the projections produced in the study, as different downscaling techniques represent the predictor–predictand relationships differently. However, in comparison to the uncertainties introduced by different GHG emission scenarios and GCMs to the projections produce by a downscaling model, uncertainties introduced by different downscaling techniques are quite limited (Sachindra *et al.*, 2014c). In statistical downscaling it is assumed that the predictor–predictand relationships derived based on past hydroclimatic data in model calibration are also valid for the future. This is called the stationarity assumption on predictor–predictand relationships. However, this assumption can become less reliable under changing climate. Therefore, the above assumption can also introduce uncertainties to the projections produced in this study. The incorporation of non-stationarity of predictor–predictand relationships into downscaling approaches has been discussed in detail in the study of Raje and Mujumdar (2010).

Also in this study, only one pair of urban and rural stations was considered for the demonstration of the methodology. However, the use of a number of urban and rural stations located in different climate zones will enable better understanding of the effectiveness of the downscaling approaches used in this study in different climate zones. Furthermore, in this study it was assumed that the size and the population of Melbourne city will remain the same in the future as in the past. This assumption aided the quantification of the impact of climate change on the intensity of Melbourne's UHI separating the influences of size and the population of the city on the UHI. However, owing to the above assumption the intensity of Melbourne's UHI computed for the future in this study could be underestimated, as with the size and the population the intensity of a UHI increases.

5. Summary and conclusions

This study was focussed on the investigation of the impacts of climate change on the urban heat island (UHI) in the central business district (CBD) of Melbourne in Australia. Also the study investigated the changes in the number of very hot days in summer and very cold days in winter in the CBD of Melbourne in the future, under changing climate. For the investigation of the intensity of the UHI in the CBD of Melbourne, the weather station located in Laverton (less urbanised area) was selected as the reference station. The difference between the minimum/maximum daily temperature in the CBD of Melbourne and Laverton was considered as the nocturnal/diurnal UHI intensity in the CBD of Melbourne. It was found that in the CBD of Melbourne the nocturnal UHI intensity shows a clear rising trend unlike the diurnal UHI intensity, over the period 1952–2010. Therefore, in this study the changes in the nocturnal UHI intensity in the CBD of Melbourne under changing climate were investigated. In this study, statistical models were developed for downscaling monthly outputs of HadCM3, GFDL2.0 and ECHAM5 pertaining to the A2 greenhouse gas (GHG) emission scenario to average monthly minimum temperature in the CBD of Melbourne and Laverton. Then using the average monthly minimum temperature projections pertaining to the above three GCMs, the monthly ensemble average minimum temperature projection was computed. Using this monthly ensemble average minimum temperature in the CBD of Melbourne and Laverton, the monthly ensemble average nocturnal UHI intensity in the Melbourne CBD was projected into the future period 2000–2099. The average of monthly ensemble minimum temperature in the CBD of Melbourne and Laverton indicated a gradual rise in all seasons over the five time slices: 2000–2019, 2020–2039, 2040–2059, 2060–2079 and 2080–2099. However, such a gradual rise in the ensemble average of nocturnal UHI intensity in the Melbourne CBD was only seen in summer over the four time slices: 2000–2019, 2020–2039, 2040–2059 and 2060–2079. Also in this study, statistical models were developed for downscaling the outputs of HadCM3, GFDL2.0 and ECHAM5 pertaining to the A2 GHG emission scenario to number of very hot days (maximum daily temperature exceeding 35 °C) in November–March and number of very cold days (minimum daily temperature below 5 °C) in May–September. It was seen that the ensemble average number of very hot days in December–March will increase gradually over the time slices 2000–2019, 2020–2039, 2040–2059, 2060–2079 and 2080–2099 in the CBD of Melbourne. Also in the CBD, during 2040–2099, the average number of very hot days in February will be higher than that of January (in the past the highest number of very hot days was seen in January). Furthermore, in March, the average number of very hot days showed an increasing trend starting from time slice 2040–2059. This is a possible indication of an expansion of the future summer weather into early autumn in the CBD of Melbourne. Also the number of very cold days in September tended to increase in the future, hinting at the expansion of winter weather to early spring in the Melbourne CBD. However, in May, June, July, and August a decrease in the number of very cold days with the rising GHG emissions was seen almost throughout the twenty-first century.

The following conclusions were also derived from this study:

1. The gene expression programming (GEP) technique can be used to develop statistical models for effectively downscaling general-circulation model (GCM) outputs to average monthly minimum temperature and also to the average number of very hot days and very cold days in calendar months. The direct downscaling of monthly GCM outputs to the number of very hot days and very cold days in calendar months avoids the need of downscaling daily GCM outputs to daily minimum/maximum temperature for the identification of the number of very hot days and very cold days in calendar months. The above procedure used in this study is quite useful, as downscaling daily GCM outputs to daily minimum/maximum temperature needs the management of large sets of input and output data to the downscaling models, which is computationally a cumbersome task.
2. Continuation of the evolution of GEP-based downscaling models caused model over-fitting in calibration and under-fitting in validation. The selection of the models which showed the best performance in validation is seen as an effective way to avoid the models which displayed over-fitting in calibration and under-fitting in validation.
3. Monthly bias-correction was very effective in reducing the bias in the statistics of monthly minimum temperature reproduced by the downscaling models when run with the twentieth-century climate experiment data of a GCM.
4. Though the rising greenhouse gas concentrations cause an elevation in temperature at both urban and less urbanised areas, the urban heat island intensity tends to increase.

This indicated that the presence of urban structures can magnify the effect of global warming at the local scale and hence intensify the urban heat island effect in cities.

Acknowledgements

The authors acknowledge the financial assistance provided by Victoria University for this project. The authors also wish to thank the editor, the associate editor and the anonymous reviewer for their useful comments, which have improved the quality of this article.

References

Akbari H, Pomerantz M, Taha H. 2001. Cool surfaces and shade trees to reduce energy use and improve air quality in urban areas. *Sol. Energy* **70**: 295–310.

Anandhi A, Srinivas VV, Nanjundiah RS, Kumar DN. 2008. Downscaling precipitation to river basin in India for IPCC SRES scenarios using support vector machine. *Int. J. Climatol.* **28**: 401–420.

Anandhi A, Srinivas VV, Nanjundiah RS, Kumar DN. 2009. Role of predictors in downscaling surface temperature to river basin in India for IPCC SRES scenarios using support vector machine. *Int. J. Climatol.* **29**: 583–603.

Anandhi A, Srinivas VV, Nanjundiah RS, Kumar DN. 2012. Daily relative humidity projections in an Indian river basin for IPCC SRES scenarios. *Theor. Appl. Climatol.* **108**: 85–104, doi: 10.1007/s00704-011-0511-z.

Arya SP. 2001. *Introduction to Micrometeorology.*, International Geophysics Series Vol. 79 (2nd edition). Academic Press: San Diego, CA.

Chen TS, Yu PS, Tang YH. 2010. Statistical downscaling of daily precipitation using support vector machines and multivariate analysis. *J. Hydrol.* **385**: 13–22.

De Souza DO, dos Santos Alvalá RC. 2012. Observational evidence of the urban heat island of Manaus City, Brazil. *Meteorol. Appl.* **21**: 186–193.

EPA. 2013. '*Reducing urban heat islands: compendium of strategies*'. http://www.epa.gov/hiri/resources/pdf/BasicsCompendium.pdf (accessed 1 February 2014).

Ferreira C. 2006. *Gene Expression Programming: Mathematical modeling by an artificial intelligence* (2nd edition). Springer-Verlag: Berlin and Heidelberg, Germany.

Fowler HJ, Blenkinsop S, Tebaldi C. 2007. Linking climate change modelling to impacts studies: recent advances in downscaling techniques for hydrological modelling. *Int. J. Climatol.* **27**: 1547–1578.

Giannaros TM, Melas D, Daglis IA, Keramitsoglou I. 2014. Development of an operational modeling system for urban heat islands: an application to Athens, Greece. *Nat. Hazards Earth Syst. Sci.* **14**: 347–358.

Giannopoulou K, Livada I, Santamouris M, Saliari M, Assimakopoulos M, Caouris Y. 2011. On the characteristics of the summer urban heat island in Athens, Greece. *Sustainable Cities Soc.* **1**: 16–28.

Haberlandt U, Belli A, Bárdossy A. 2014. Statistical downscaling of precipitation using a stochastic rainfall model conditioned on circulation patterns – an evaluation of assumptions. *Int. J. Climatol.* **35**: 417–432, doi: 10.1002/joc.3989.

Hajat S, O'Connor M, Kosatsky T. 2010. Health effects of hot weather: from awareness of risk factors to effective health protection. *The Lancet* **375**: 856–863.

Hashmi MZ, Shamseldin AY, Melville BW. 2011. Statistical downscaling of watershed precipitation using Gene Expression Programming (GEP). *Environ. Modell. Software* **26**: 1639–1646.

Hassan Z, Shamsudin S, Harun S. 2014. Application of SDSM and LARS-WG for simulating and downscaling of rainfall and temperature. *Theor. Appl. Climatol.* **116**: 243–257.

Hoffmann P, Krueger O, Schlünzen KH. 2012. A statistical model for the urban heat island and its application to a climate change scenario. *Int. J. Climatol.* **32**: 1238–1248.

Howard L. 1833. *The Climate of London*, **I-III**. Harvey and Darton: London.

IPCC. 2007. Climate change 2007: Synthesis report. In *Contribution of Working Groups I, II and III to the Fourth Assessment Report of the Intergovernmental Panel on Climate Change*, Pachauri RK, Reisinger A. (eds.) IPCC: Geneva, Switzerland. http://www.ipcc.ch/publications_and_data/publications_ipcc_fourth_assessment_report_synthesis_report.htm (accessed 1 February 2014).

Jay O, Kenny GP. 2010. Heat exposure in the Canadian workplace. *Am. J. Ind. Med.* **53**: 842–853.

Jin MS. 2012. Developing an index to measure urban heat island effect using satellite land skin temperature and land cover observation. *J. Climate* **25**: 6193–6201.

Johnson F, Sharma A. 2012. A nesting model for bias correction of variability at multiple time scales in general circulation model precipitation simulations. *Water Resour. Res.* **48**: 1–16.

Jones PD, Wigley TML, Wright PB. 1986. Global temperature variations between 1861 and 1984. *Nature* **332**: 430–434.

Karl TR, Wang WC, Schlesinger ME, Knight RW, Portman D. 1990. A method of relating general circulation model simulated climate to the observed local climate Part I: Seasonal statistics. *J. Climate* **3**: 1053–1079.

Livada I, Santamouris M, Assimakopoulos M. 2007. On the variability of summer air temperature during the last 28 years in Athens. *J. Geophys. Res.* **112**: D12103, doi: 10.1029/2006JD008140.

McCarthy JJ. 2009. Reflections on: our planet and its life, origins, and futures. *Science* **326**: 1646–1655.

Mares C, Mares I, Huebener H, Mihailescu M, Cubasch U, Stanciu P. 2014. A hidden Markov model applied to the daily spring precipitation over the Danube basin. *Adv. Meteorol.* **2014**: 237247, doi: 10.1155/2014/237247.

Morris CJG, Simmonds I. 2000. Associations between varying magnitudes of the urban heat island and the synoptic climatology in Melbourne, Australia. *Int. J. Climatol.* **20**: 1931–1954.

Oke TR. 1973. City size and the urban heat island. *Atmos. Environ.* **7**: 769–779.

Oke TR. 1987. *Boundary Layer Climates* (2nd edition). Methuen: London.

Oke TR. 1988. The urban energy balance. *Prog. Phys. Geogr.* **12**: 471–508.

Peng S, Piao S, Ciais P, Friedlingstein P, Ottle C, Bréon FM, Nan H, Zhou L, Myneni RB. 2012. Surface urban heat island across 419 global big cities. *Environ. Sci. Technol.* **46**: 696–703.

Raje D, Mujumdar PP. 2010. Constraining uncertainty in regional hydrologic impacts of climate change: nonstationarity in downscaling. *Water Resour. Res.* **46**: W07543, doi: 10.1029/2009WR008425.

Sachindra DA, Huang F, Barton AF, Perera BJC. 2014a. Statistical downscaling of general circulation model outputs to precipitation. Part 1: Calibration and validation. *Int. J. Climatol.* **34**: 3264–3281, doi: 10.1002/joc.3914.

Sachindra DA, Huang F, Barton AF, Perera BJC. 2014b. Statistical downscaling of general circulation model outputs to precipitation. Part 2: Bias-correction and future projections. *Int. J. Climatol.* **34**: 3282–3303, doi: 10.1002/joc.3915.

Sachindra DA, Huang F, Barton AF, Perera BJC. 2014c. Statistical downscaling of general circulation model outputs to catchment scale hydroclimatic variables: issues, challenges and possible solutions. *J. Water Clim. Change* **5**: 496–525, doi: 10.2166/wcc.2014.056.

Sachindra DA, Huang F, Barton AF, Perera BJC. 2014d. Potential improvements to statistical downscaling of general circulation model outputs to catchment streamflows with downscaled precipitation and evaporation. *Theor. Appl. Climatol.*, doi: 10.1007/s00704-014-1288-7.

Salvi K, Kannan S, Ghosh S. 2011. 'Statistical downscaling and bias-correction for projections of Indian rainfall and temperature in climate change studies'. In *Proceedings of 4th International Conference on Environmental and Computer Science*, 16–18 September 2011. IPCBEE **19**: 7–11. IACSIT Press: Singapore.

Schlunzen KH, Hoffmann P, Rosenhagen G, Riecke W. 2010. Long-term changes and regional differences in temperature and precipitation in the metropolitan area of Hamburg. *Int. J. Climatol.* **30**: 1121–1136.

Smith I, Chandler E. 2009. Refining rainfall projections for the Murray Darling basin of south-east Australia – the effect of sampling model results based on performance. *Clim. Change* **102**: 377–393.

Tan J, Zeng Y, Tang X, Guo C, Li L, Song G, Zhen X, Yuan D, Kalkstein AJ, Li F, Chen H. 2010. The urban heat island and its impact on heat waves and human health in Shanghai. *Int. J. Biometeorol.* **54**: 75–84.

Timbal B, Fernandez E, Li Z. 2009. Generalization of a statistical downscaling model to provide local climate change projections for Australia. *Environ. Modell. Software* **24**: 341–358.

Tisseuil C, Vrac M, Lek S, Wade AJ. 2010. Statistical downscaling of river flows. *J. Hydrol.* **385**: 279–291.

Torok SJ, Morris CJG, Skinner C, Plummer N. 2001. Urban heat island features of southeast Australian towns. *Aust. Meteorol. Mag.* **50**: 1–13.

Wilby RL. 2003. Past and projected trends in London's urban heat island. *Weather* **58**: 251–260.

Willems P, Vrac M. 2011. Statistical precipitation downscaling for small-scale hydrological impact investigations of climate change. *J. Hydrol.* **402**: 193–205.

Yow DM. 2007. Urban heat islands: observations, impacts, and adaptation. *Geogr. Compass* **1**: 1227–1251.

Zakšek K, Oštir K. 2012. Downscaling land surface temperature for urban heat island diurnal cycle analysis. *Remote Sens. Environ.* **117**: 114–124.

